ASSESSMENT OF THE CRACK RESISTANCE BEHAVIOUR OF MARTENSITIC STEELS BY FRACTURE TOUGHNESS AND IN SITU TENSILE TESTS

D. Regener* and E. Schick*

This paper investigates the crack resistance of the steel P91 and its tungsten-alloyed variant E911 by fracture toughness and in situ tensile tests. Special attention is paid to the behaviour of the weld joints. In spite of uniform tempered martensitic microstructure the investigations reveal a higher crack sensitivity of the variant E911. The evaluation of pre-cracked in situ tensile specimens shows that the resistance of base, weld and heat affected metal to crack propagation is similar. However, because of the inhomogenous heat affected zone an enhanced scattering of the measured values has to take into consideration. The test temperature of 600 °C results in a reduced load carrying capability and deformability, which are often accompanied by microcracking besides and in front of the main crack.

INTRODUCTION

The pursuit of higher efficiency of power plants and thereby the reduction of harmful emissions in the environment has led to the development of new more creep resistant 9-12 % chromium steels providing also sufficient resistance to corrosion and oxidation. This material group includes the steel X 10 CrMoVNb 9-1 (P91) and its tungsten-alloyed variant E911. The first material applied in steam generating systems was already intensively investigated in regard to its microstructure and creep behaviour (Brühl et al (1), Bendick et al (2), Hahn et al (3), Maile et al (4) and Cadek et al (5)). Present, more attention is given to the steel E911 developed to enhance the creep strength in order to obtain reliable estimates of its long-term behaviour (Hald (6), Bendick and Ring (7)).

This paper concerns with the assessment of the resistance of the steels P91 and E911 and their matched weld joints to crack propagation. Furthermore, the influence of a 1000 h - annealing at 600 °C on the deformation and fracture behaviour of the investigated steel P91 is shown. Special attention is paid to the weld joint (comprising of base, weld and heat affected zone (HAZ)) often considered to be a life-limiting factor.

* Otto-von-Guericke-University Magdeburg, Germany

EXPERIMENTAL

The chemical composition of the investigated steels is presented in Table 1. The contents of the elements are in accordance with the recommendations.

TABLE 1 - Chemical Composition of the used Materials (%)

	C	Si	Mn	P	S	Cr	Ni	Mo	V	Nb	W	N
P91	0.09	0.32	0.44	0.019	0.006	8.45	0.25	0.90	0.19	0.064		0.039
E911	0.10	0.14	0.52	0.023	0.016	8.20	0.30	0.95	0.18	0.057	0.91	0.071

The initial state of the steel P91 resulted from austenitisation at 1050 °C 10 min / air cooling, tempering at 750 °C 70 min / air cooling. Furthermore, this steel was long-term annealed at 600 °C 1000 h. The heat treatment of the steel E911 occurred by austenitisation at 1050 °C 30min / air cooling, tempering at 760 °C 60 min / air cooling. The welding pad of the same composition as the base P91 was prepared by a manual electrode welding (regarding the root pass) and manual TIG welding. The circumferential weld of the pipe from E911 occurred by manual arc welding. The postweld heat treatment was performed at 770 °C (P91) and at 750 °C (E911) 4h / air cooling, respectively.

The microstructural investigation of the materials revealed a tempered martensitic lath structure with carbides chiefly arranged on the former austenite grain boundaries and lath boundaries. The long-term annealing of the steel P91 became apparent by more homogeneity of the grain structure without to change clearly the mechanical properties. These properties were mainly determined on longitudinal specimens taken along the pipe direction. Additional measurements on specimens taken transversal to the pipe direction show only clear differences in the Charpy toughness (Table 2).

TABLE 2 - Mechanical Properties of the used Materials

	P91 (initial state)		P91 (annealed state)	E911 (initial state)	
	longitudinal	transversal	longitudinal	longitudinal	transversal
$R_{p0.2}$ (N/mm^2)	543	531	473	542	
R_m (N/mm^2)	682	723	651	725	
A (%)	13	15	18	16	
Z (%)	68	71	70	61	
A_V (J)	201	127	199	163	101
HV10	214		216	222	

To assess the crack resistance behaviour of base materials, J-Δa-curves were determined under static and dynamic impact loading using fatigue pre-cracked Charpy specimens. Under consideration of the small dimension of the HAZ (width ≈ 4 mm), further investigations were performed by means of SEM-in situ tensile tests at room temperature

and 600 °C. To this purpose, special in situ tensile specimens (gauge length ≈ 5 mm, thickness ≈ 1mm) were pre-cracked (a/W ≈ 0.5) in such a way, that the crack tip lay in the base metal, weld metal or HAZ. All in situ tests were carried out at constant strain rate of 0.5 µm/s.

RESULTS AND DISCUSSION

In relation to the base materials, the investigations showed that the blunting and crack initiation occur in the same manner. However, distinct differences exist in regard to the crack propagation. For the sake of clarity, Figure 1 contents only the J-Δa-curves of the steel E911 and of the annealed state of P91, which reflects a more homogeneous microstructure than the initial state. Compared with P91, the steel E 911 reveals a reduced crack resistance and a higher sensitivity to the kind of loading, too. Whilst the dynamic and static crack resistance values of E911 follow two separate curves, the J-Δa-values of P91 are superimposed. The determination of the initiation toughness J_i on the base of measurements of stretch zone width was very difficult, because this region was highly uneven along the thickness of specimens. In addition, numerous secondary cracks complicated the measurements. Therefore, the so determined J_i-values (P91d,a = 200 N/mm, P91s,a = 190 N/mm, E911d = 110 N/mm, E911s = 105 N/mm) do not represent guaranteed values.

In situ tensile tests on unnotched specimens of the base materials provide at room temperature maximum stresses, which are similar to the scale of the required ultimate tensile strength (e.g. E911, Fig. 2). The measured fracture strains exceed considerably the values determined by usual tensile tests due to the small dimensions of specimens. Therefore, they serve only to the comparison of the material behaviour characterised by the in situ tests. An essential decrease of maximum stress and fracture strain occurs owing to higher test temperature. The direct SEM-observation of the deformation process showed that cavities form and grow in the necked region at reduced strain values. Preferred sites of first cavities are inclusions and carbides on former austenite boundaries.
The strength of weld metal is partly higher as that of base metal without noticeable reduction of strain. This is also in correlation with the hardness HV10 measured across the weld. The hardness of the weld metal exceeds that of base metal by about 10 units. However, due to a more inhomogeneous microstructure the strength values of weld metal scatter stronger (Fig. 2).

The investigations of fatigue cracked in situ tensile specimens made possible the comparison of the crack resistance behaviour of base metal, weld metal and HAZ.
Figure 3 shows stress-elongation curves of the investigated base materials. To document the geometry- and microstructure-induced scattering, each material is represented by a curve with the highest and lowest measured values. Regarding the initial state of P91, the wide scattering is attributed to the inhomogeneity of the material due to the short austenitising time. An improvement of the homogeneity has been achieved by the 1000 h long-term annealing at 600 °C without to reduce essentially the strength (Table 2). The observation of the microstructure by SEM revealed a frequent branching of the initial fatigue

cracks developing along disturbed regions like grain and lath boundaries in all investigated materials. During the loading the crack tip blunts strongly due to the high deformability of the material. According to the reduced stress intensity on the blunted tip the remaining cross section of the specimen is able at first to bear such high stress, which is comparable to that in an unnotched specimen. Crack nuclei form in highly deformed regions ahead of the crack front. In particular, along the shear bands microcracking occurs at an angle of ≈ 45 °. The stable propagation of the main crack fulfils by repeated initiation, growth and blunting.

Comparing the stress-elongation curves of base, weld and heat affected material of P91 (Fig. 4), it is obvious that the maximum stresses of base and weld metal can achieve similar high values. The higher test temperature of 600 ° decreases both the load carrying capability and the deformability of the microstructure in all regions of weld joint. The reduced deformability becomes apparent by increasing microcracking besides and in front of the main crack. This appearence is chiefly observed in heat affected material.
Because for the sake of clarity Figure 4 presents only selected curves, a certain scattering of the material behaviour has to take into consideration. In particular, this can be related to the heat affected material, because the hardness profile taken across the weld joint shows clear variations. Due to different microstructure the extent of the variations amounts up to 30 HV10-units. The highest value was found near the weld metal and the lowest near the base metal, respectively.

REFERENCES

(1) Brühl, F., Haarmann, K., Kalwa, G., Weber, H. and Zschau, M., VGB Kraftwerkstechnik, Vol. 69, No. 12, 1989, pp. 1214 - 1224.

(2) Bendick, W., Rasche, C., Haarmann, K. and Zschau, M., 3R international, Vol. 32, No. 9, 1993, pp. 494 - 499.

(3) Hahn, B., Baumhoff, V., Peters, K. and Zschau, M., VGB Kraftwerkstechnik, Vol. 77, No. 7, 1997, pp. 214 - 220.

(4) Maile, K., Theofel, H., Bendick, W. and Zschau, M., Stahl und Eisen, Vol. 117, No. 8, 1997, pp. 101 - 105.

(5) Cadek, J., Sustek, V. and Pahutova, M., Mater. Sci. & Engng, Vol. A225, 1997, pp. 22 - 28.

(6) Hald, J., steel research, Vol. 67, No. 9, 1996, pp. 369 - 374.

(7) Bendick, W. and Ring, M., steel research, Vol. 67, No. 9, 1996, pp. 382 - 385.

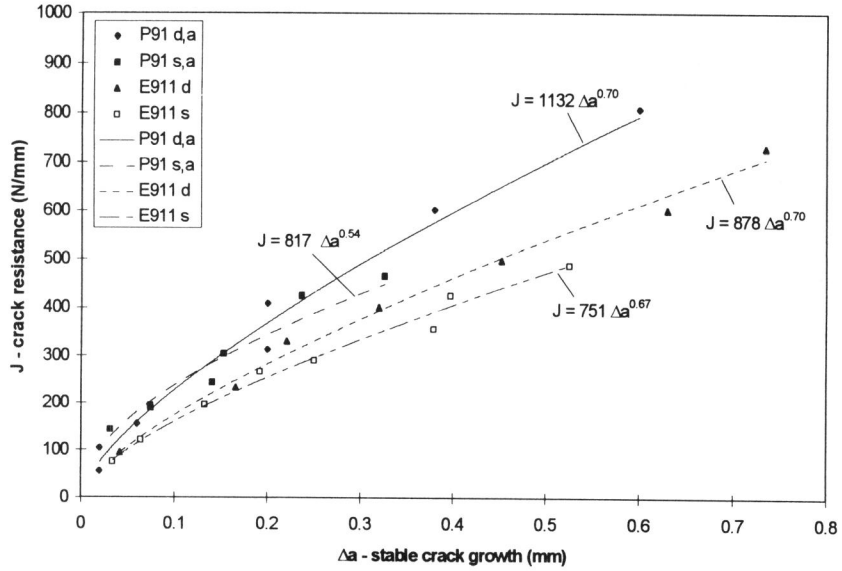

Figure 1 Static (s) and dynamic (d) crack resistance curves of the materials P91 (annealed state (a)) and E911

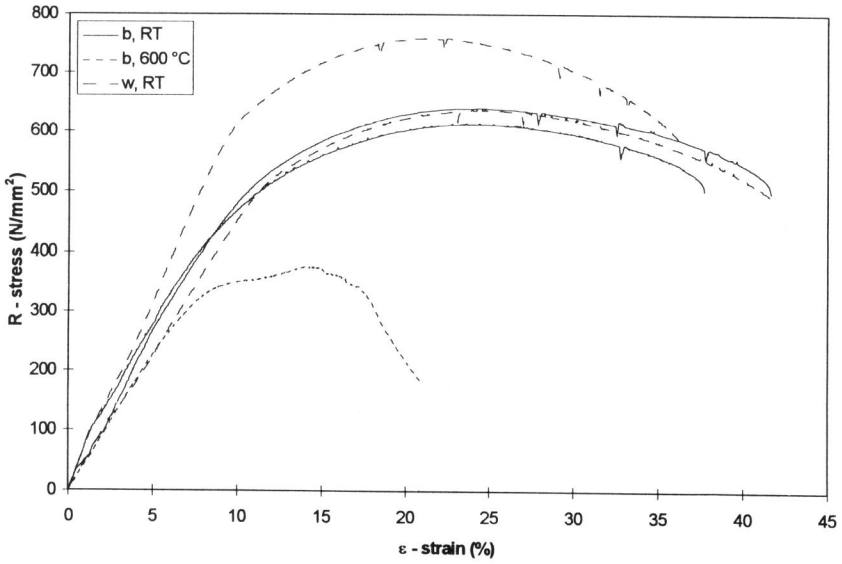

Figure 2 In situ stress-strain curves of base (b) and weld (w) material of E911

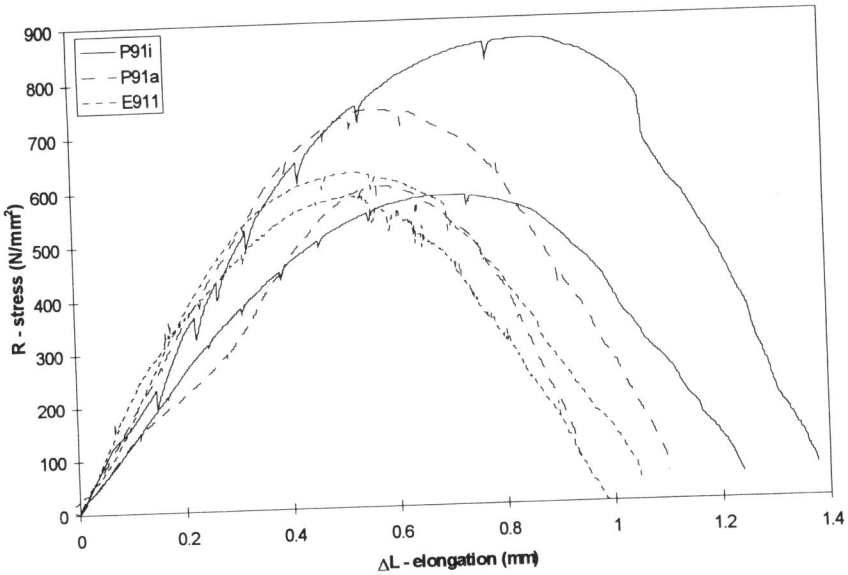

Figure 3 Stress-elongation curves obtained of fatigue cracked in situ specimens of the materials P91 [initial (i) and annealed (a) state] and E911

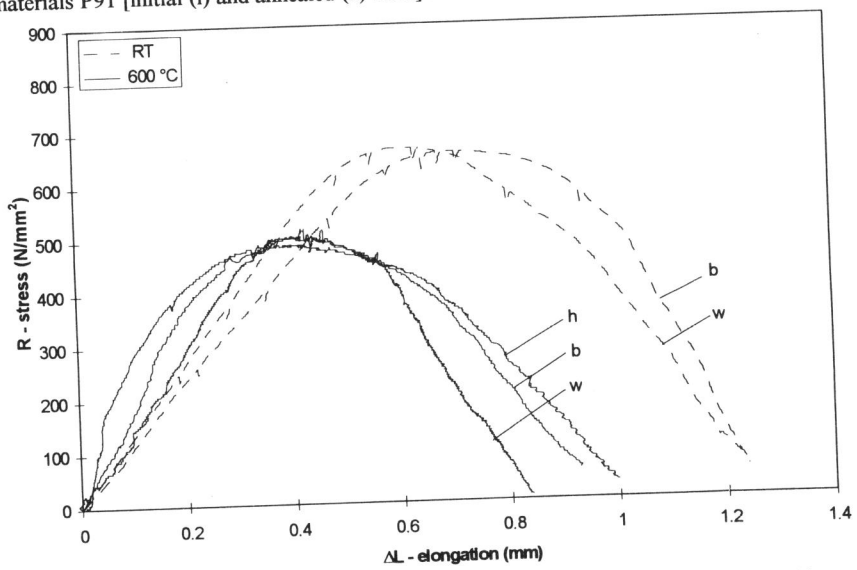

Figure 4 Stress-elongation curves obtained of fatigue cracked in situ specimens of base (b), weld (w) and heat affected (h) material of P91